Mechanics and Mechanical Engineering
Vol. 21, No. 1 (2017) 67–83

Numerical Study of the Mechanical Behavior and Fatigue in a Weld Bead by Friction Stir for a 6082–T6 Aluminum Alloy

Youb Kambouz
Mohamed Benguediab
Benattou Bouchouicha
Laboratory of Material and Reactive System
Departement of Mechanical Engineering
University of Sidi Bel–Abbes
Sidi Bel–Abbes, Algeria
y_kambouz@yahoo.fr

Received (12 October 2016)
Revised (16 November 2016)
Accepted (21 December 2016)

The process of friction stir welding is a significant advance in the field of research on the Friction welding technique known for several decades. This assembly technique has obvious originality since welding is performed in the solid state, which can help eliminate birth defects related to solidification phase compared to conventional welding.
The numerical modeling of this type of process is complex, not only in terms of the variety of physical phenomena which must be considered, but also because of the experimental procedure that must be followed in order to verify and validate numerical predictions. In this work, a finite element model is proposed in order to simulate the crack propagation under monotonic loading in different areas of the weld seam of a specimen CT–50 aluminum alloy 6082–T6.
Microhardness tests were performed to characterize the Vickers hardness profile in the vicinity of the weld area. Friction stir welding process leads to a decrease of the static mechanical properties relatively to base material. Detailed examination revealed a hardness decrease in the thermo mechanically affected zone and the nugget zone average hardness was found to be significantly lower than the base alloy hardness. Welded specimens show significantly lower lives than base material.

Keywords: FEM, weld bead, friction welding.

1. Introduction

Considered as the most significant development in metal joining in the last decade, the Friction Stir Welding (FSW) is a joining process with good energy efficiency that is also environmentally friendly and versatile. Significant research has been conducted in various fields since the invention of this technique in 1991, [1]. Generally, FSW specimens have higher resistance than specimens welded using the Metal

Inert Gas (MIG) and Tungsten Inert Gas (TIG) processes. [2] and [3], compared fatigue results of friction stir welds with data obtained for conventional arc-welding methods, namely, MIG–pulse and TIG processes in aluminum alloy (T6 and T4 conditions). [4, 5] also compared the fatigue behaviour of joints performed by the traditional MIG welding process and by the FSW process, observing that FSW and MIG welded specimens had lower yield and ultimate stresses than the base material. In general, a higher lifetime for the friction stir welds in comparison with other welds was also observed by [6]. It has also been observed that FSW leads to a decline of the mechanical properties of weld bead in comparison to the base metal [7]. Furthermore, an important hardness decrease in the Thermomechanically Affected Zone (TMAZ) and a nugget zone average hardness was recorded.
Due to severely thermal and mechanical deformation in the weld zone during FSW, this zone generally possesses various microstructural features and various mechanical properties [8] and [9]. The crack propagation in the weld bead (FSW and classic) is known to be concerned by residual stress and/or hardness around the welded zone [10] and [11]. [12] Conducted hardness tests on micro-specimen.
The limit of elasticity, tensile strength and Young's modulus (E) of the aluminum alloy (6082-T6) were measured using tensile tests on welded and non-welded specimens.
Modeling the tensile behavior of welded FSW for an aluminum alloy joint showed that the weak area is the HAZ, [13]. Welding parameters also affect the mechanical properties of the weld and its resistance is related to the speed of rotation of the welding tool [14] and [15]. It is therefore advisable to choose the best parameters speed, welding speed and good fixation of the parts [16].

2. Presentation of the material

The material used is an aluminum alloy 6000 series subjected to T6 treatment, which will help the investigation of the various phenomena that occur during welding with involving the precipitation phenomenon.
This aluminium alloy is a high strength Al–Mg–Si alloy that contains manganese to increase ductility and toughness. The T6 condition is obtained through artificial ageing at a temperature of approximately 180°C [2].
The alloy chemical composition and mechanical properties are shown in Tables 1 and 2, respectively.

Table 1 Chemical composition of AA 6082-T6 aluminum alloy (wt %)

Si	Mg	Mn	Fr	Cr	Cu	Zn	Ti	Al
1.3	1.2	1.0	0.5	0.25	0.1	0.2	0.1	98.3

Table 2 Tensile properties for base materials [17]

Material	E[MPa]	σ_e[MPa]	σ_{max}[MPa]	ε[%]	n	K[MPam$^{1/2}$]
Al6082T6	69000	260	366	13.3	0.10	22

2.1. *Hardness profile and microstructure of the 6082–T6 FSW joint*

The optimization of the weld process requires the mechanical characterization of the weld bead. The most commonly used practice is the measurement of microhardness which gives a first evaluation of the mechanical properties in different areas of the weld, in order to obtain a profile across it and to establish the weld zones. The cross–section thus provides a profile of microhardness [18]. The Vickers hardness profiles for all areas (BM, HAZ, TMAZ and nugget) are presented in Fig. 1. A hardness decrease occurs when approaching the TMAZ. The average hardness of the nugget zone (NZ) was found to be significantly lower than the hardness of the base alloy. There is a zone outside the nugget (transition between TMAZ and HAZ) which has the lower hardness value. In [19] and [20], it is suggested that the variation of the microhardness values in the welded area and parent material is due to the difference between the microstructures of the base alloy and weld zone.

In the tensile tests of the dissimilar specimens it was observed that the fracture surface is coincident with this zone of lower values of hardness.

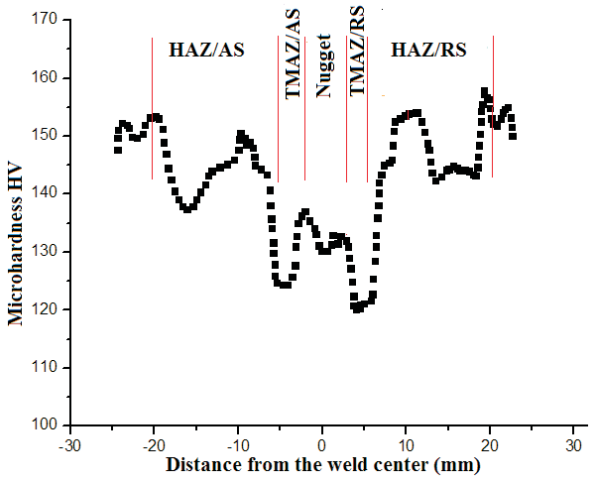

Figure 1 Hardness profile

Pictures of the microstructure of the different areas of the 6082-T6 alloy aluminum can be found in [21].

An recrystallization was observed in nugget. By moving towards the BM, no re-crystallization was observed in TMAZ and in HAZ.

Optical micrographs of the thin friction stir welded joint are illustrated in Figs. 2. The weld exhibits distinct regions as shownin on these figures.

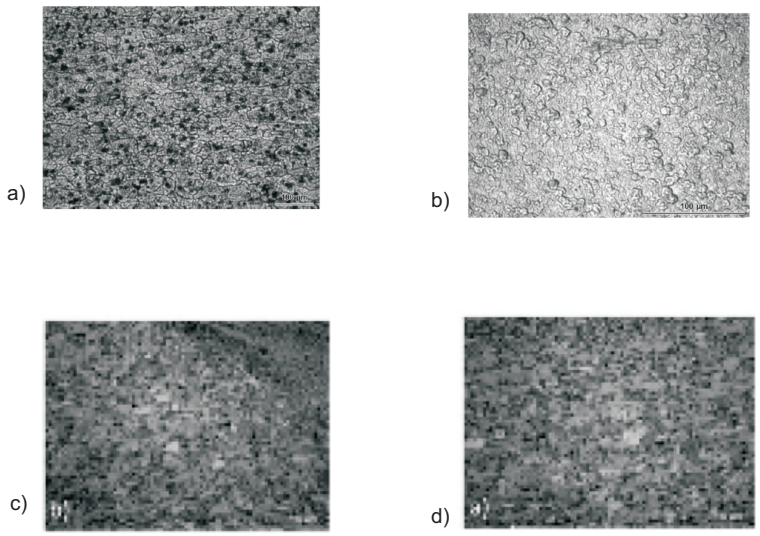

Figure 2 The Base Material (or parent material), HAZ, TMAZ and Nugget for the 6082-T6 [21]: a) Grains of base material, b) Nugget with its fine recrystallized grains, c) Grains of TMAZ, d) Grains of HAZ

2.2. *Numerical protocol and mechanical properties of the material*

The tensile test is modeled and simulated in the calculation software Abaqus FEA. This step requires the setting of many sizes and choices in the model which are explained in this study.

A displacement along the axis "y" is imposed. A fault is inserted to initiate and locate the break.

The numerical method was performed using standard rectangular tension test specimens [22], Fig. 3.

The geometry of the specimen is created under the 2D software. Geometry and boundary conditions are defined in Fig. 4.

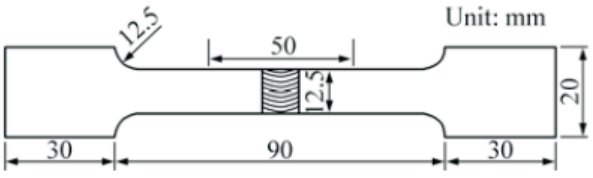

Figure 3 Tensile specimen

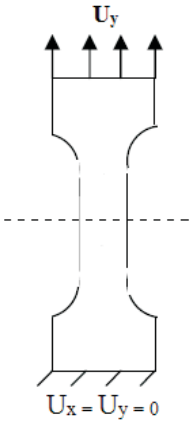

Figure 4 Geometry and boundary conditions in the simulation of a tensile test

The calculations are made in explicit because the removal of the elements is managed directly by Abaqus. The explicit approach depends on the size of the mesh.
By refining the mesh, the calculation time increases. It is therefore preferable to use a coarse mesh. However, it is also necessary to refine the crack tip mesh to visualize phenomena such as plasticity.
FSW joints in 6082–T6 aluminium alloys of 6 mm in thickness were subjected to a number of tensile tests. The aim of this work is to gain some understanding on mechanical properties and on the effect of plastic deformation on the microstructure of thin aluminium alloy FSW joints.
Fig. 5 shows a broken test specimen under Abaqus software.
Tab. 3 presents the tensile properties for friction stir welded specimens and base material.
A softening of the material is observed in the weld region. This softening is most evident in the heat affected zone of the welds and corresponded to the failure location in tensile tests. The reason for this phenomenon was the kinetic and thermal asymmetry of the FSW process. An initial stage of a longitudinal, volumetric defect was found at the intersection of weld nugget and thermomechanically affected zone. The test results from the 6082–T6 welds are lower than the parent material due to thermal softening. This caused final failure through the heat affected zone (HAZ) for both the flaw–free and the flawed welds, although failure of the flawed weld originated from the weld root. Both the flaw-free and the flawed welds had similar proof strengths but the flawed weld exhibited significantly lower tensile strength and ductility.
Results of tensile tests simulation on unwelded and welded samples, performed in this paper, are here mentioned in table 3, these tests showed a remarkable reduction of both tensile strength (from ∼320 MPa down to 200 MPa) and elongation (from ∼ 16% down to ∼ 7%) as compared with nominal
The hardness of heat affected zone (HAZ) and Thermo- mechanically Affected Zone (TMAZ) is lower than that of base metal (BM).This difference between HAZ and

TMAZ is attributable to the partial recrystallization of the grains in the TMAZ caused by stirring. The softest points of the joints correspond to the failure locations in tensile tests.

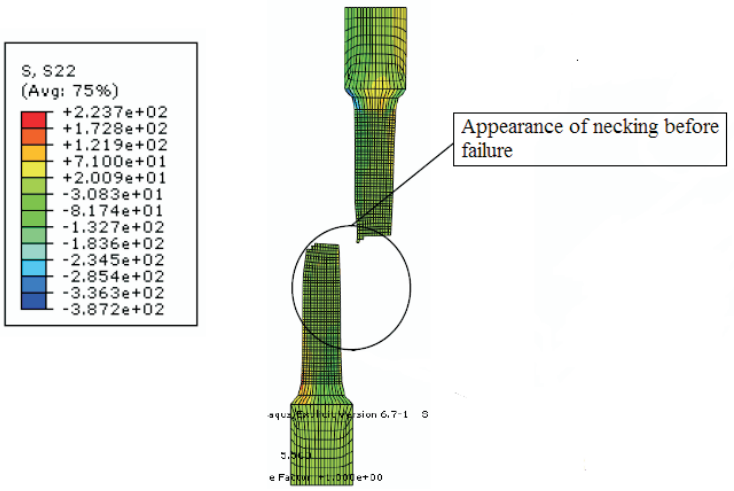

Figure 5 2D simulation of a tensile test. S_{22} constraints after the failure

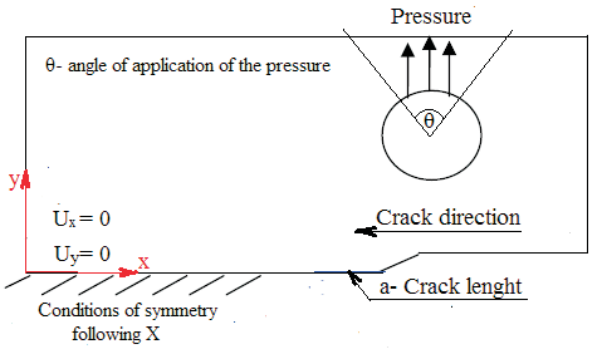

Figure 6 Modeling of the specimen CT-50 and boundary conditions

For each set of welding parameters, local tensile strength and local ductility vary widely. In turn, variations in these local conditions result in different bulk tensile strengths and bulk ductility. The lowest Tensile Strength found for welds in FSW for 6082-T6 was 64% of the base metal strength. This variety suggests that parameters can be tailored in order to impart desired weld characteristics.

Table 3 Results of tensile tests on unwelded and welded samples

N^o	Sample	Tensile strengh [MPa]	Zones of rupture	Elongation [%]	Hardness [Hv]
1	Base material	322.6	BM	16.8	110
2	Base material	323.4	BM	15.2	
3	Base material	322.7	BM	16.5	
-	Average	322.9	BM	16.2	
1	As welded	286	Nugget	10.8	78 to 84
2	As welded	279	Nugget	10.4	-
3	As welded	218	HAZ/ TMAZ	7.5	-
4	As welded	221	HAZ/ TMAZ	8.6	-
5	As welded	230	HAZ/ TMAZ	8.4	-
6	As welded	225	HAZ/ TMAZ	8.7	75 to 85
7	As welded	211	HAZ	7.4	65 to 109
8	As welded	207	HAZ	7.0	-
9	As welded	213	HAZ	7.3	-
10	As welded	209	HAZ	7.2	65 to 109

3. Modeling of the specimen CT-50

The calculations are made in two dimensions to meet the time constraint. Similarly, only half CT50 specimen is modeled.

3.1. *Modeling of the cracked part*

The modeled weld is divided into several zones, as shown in Fig. 7, and a different mechanical behavior is assigned for each.

In the model considered in this paper, the areas are fully supportive of each other, movement is continuous and normal stress is transmitted. This model allows the obtainment of a mapping of local deformations through a welded joint (Fig. 8). The part is a CT–50 specimen, the cracking plane is considered normal to the loading axis and the crack front is considered straight.

Table 4 Material parameters entered in Abaqus

	6082-T6	6082-T6 (FSW)
E [MPa]	68000	51200
R_p [MPa]	265	135.8
C [MPa]	1100	1100
s	0.93	0.93
S [MPa]	2	2

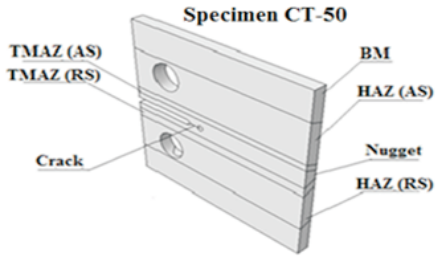

Figure 7 Representation of welding areas

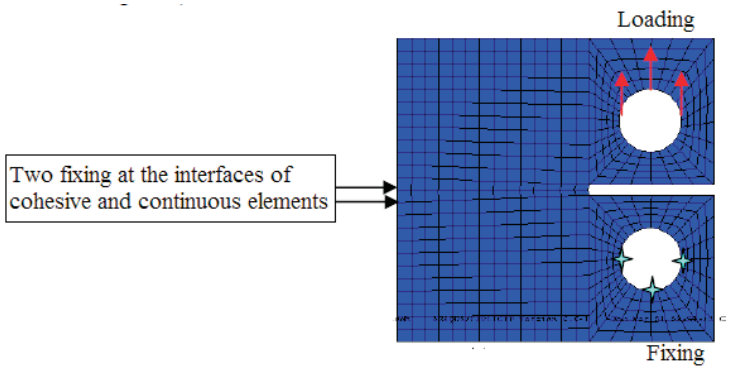

Figure 8 Cohesive elements and boundary conditions

3.2. *Mesh of the cracked part and boundary conditions*

The numerical analysis of the mechanical fields of a cracked part is strongly linked to the meshing quality of this part, particularly the vicinity of the crack tip. It is therefore important to manage the mesh to the crack tip Fig. 9.
The master surface is coarsely meshed and corresponds to the continuous elements. The slave surface is finely meshed and corresponds to the cohesive elements.

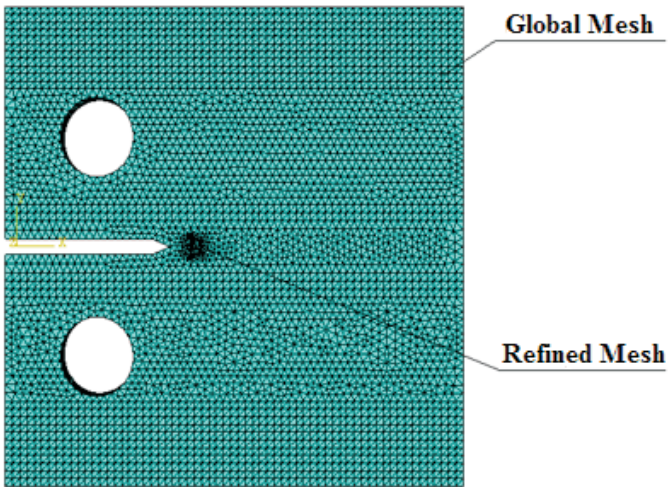

Figure 9 Mesh of the specimen

4. Numerical results

4.1. *Numerical modeling*

The simulation is performed by explicit. A specimen test CT–50 is modeled in computing software by finite element. The geometry of the specimen and the modeled conditions limits applied are shown in Figs. 7 and 8.

The mesh is refined only at the crack tip for limit the duration of the calculation. In this area, the mesh size is between 10^{-3} and 10^{-2} mm.

Loading F obeys a sinusoidal law inserted under the software as periodic amplitude:

$$\mathrm{F} = \mathrm{F_{sta}} + \mathrm{F_{amp}} \sin(2\pi \mathrm{ft}) \tag{1}$$

The values of $\mathrm{F_{stat}}$ and $\mathrm{F_{amp}}$ are related to R = 0.1, charge ratio.

Upload is modeled by a pressure P, defined on the upper surface of the hole of the CT test piece, as shown in Fig. 8.

It is introduced in two stages during the calculation. In the first "Step" static F_{sta} is applied. Then the cyclic loading is superimposed in a second "Step".

This division is necessary because the calculation converges difficult if the loads are applied simultaneously. Similarly, the frequency should not be too high because otherwise the explicit calculation diverges or the energy criterion, $\mathrm{E_{Kinetic}} << \mathrm{E_{internal}}$, ensuring the validity of the results is not checked. The choice of timing parameters take into account the convergence calculations, the energy criterion, and the need for acceptable calculation times.

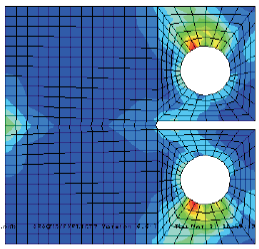

The load is applied gradually. The crack does not spread.

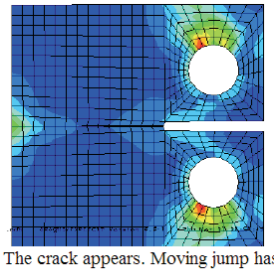

The crack appears. Moving jump has reached the critical value.

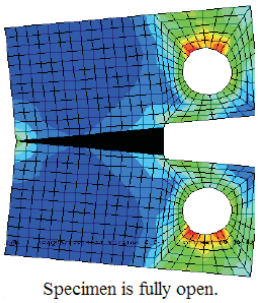

Specimen is fully open.

Figure 10 Visualization of the crack propagation

4.2. *Visualization of the crack propagation*

More than a failure criterion may be associated with calculation. A criterion consists of two stages, the initiation and propagation:

- Initiation:

  This step corresponds to the beginning of the damage. It starts when the stresses and deformations satisfy an initiation test. This phase is in no way associated with a law of propagation and does not model the damage process.

- Evolution of damage:

  A damage evolution law describes the percentage of degradation of the material in the thickness when the initiation criterion is reached. A variable D, characterizing damage and actual nominal stresses is introduced:

4.3. *Numerical determination of the curve* $\mathbf{da/dN = f(\Delta K)}$

The first objective is to compare the curves of Wohler for the different areas of welding FSW.
The Wohler curves reach clear differences between 6082–T6 (BM) and Nugget, TMAZ and HAZ. The comparison of curves (SN) characteristics of welded joints by FSW and those of the base material shows that the fatigue strength of welded joints is significantly smaller than the base material except for a few points in the areas of medium lives (Fig. 11).
Fatigue results obtained in this work are close with data obtained by other authors [23] for this welding process FSW.

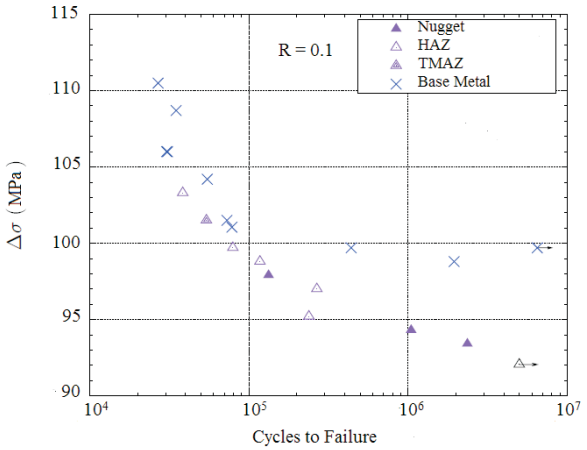

Figure 11 Fatigue endurance curves for the joints welded and base metal

The second objective is not to simulate the crack propagation test for strong ΔK, but to digitally generate the da / dN curve according to ΔK. Therefore, we opted for a stepwise approach. This method consists of performing several simulations at different values of ΔK for determining the speed of propagation of the da / dN corresponding crack at these points. For varying the value of ΔK, the length of the initial crack is changed between each simulation.

$$K = \frac{F\left(2 + \frac{a}{W}\right)}{BW^{1/2}\left(1 - \frac{a}{W}\right)^{3/2}} f\left(\frac{a}{W}\right) \tag{2}$$

$$f(a/w) = 0.886 + 4.64a/w - 13.32(a/w)^2 + 14.72(a/w)^{-3} - 5.6(a/w)^4 \tag{3}$$

F – is the applied load [N],
W – is the width of the specimen from the loading axis [m],
B – is the thickness of the test specimen [m],
a – is the crack length.

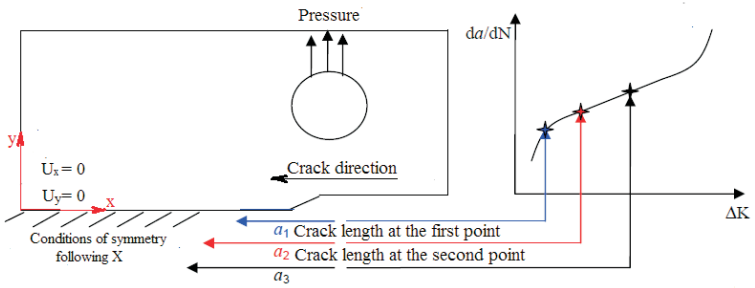

Figure 12 Obtaining of the da/dN – ΔK curve with the point by point method

For $0.2 < \frac{a}{w} < 0.3$ function, $f\left(\frac{a}{w}\right)$ established by Neuman [12] is of the form:
The propagation velocities of Crack in a 6082-T6 alloy in the different areas of the same weld (Nugget, TMAZ and HAZ) for a load ratio R = 0.1 for a specimen C (T). From the curves da/dN = ΔK (Fig. 13), several outcomes can be identified.

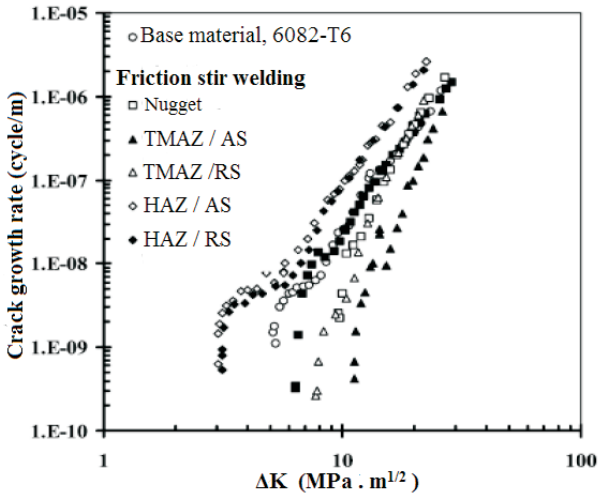

Figure 13 Crack length according to number of cycles

Studies report that the introduction of a plastic strain of 2% parallel to the joint makes the propagation speed of the same level as that of the base metal [23]. The resulting residual stresses than 2% plastic deformation did not affect hardness. Thus, the velocity of propagation will be primarily related to the distribution of residual stresses.

The rate of propagation of fatigue cracks depends on the ratio R (minimum/maximum stress). The presence of residual stresses in the bead welded changes the ratio [24] report that, in the longitudinal direction, the residual stresses are in tension. They are of + 75 MPa in the nugget and +100 MPa in the HAZ. In the transverse direction, the residual stresses are also in tension. They are of +30 MPa in the nucleus and +40 MPa in the HAZ. The crack propagation fatigue tests performed by [25] show that the rate of spread in the nugget, the HAZ and base metal for AA2024-T351 vary more in the longitudinal direction than in the direction cross. In addition, they report that the longitudinal fatigue crack growth threshold in the HAZ is about 10 MPa $m^{1/2}$, compared to 5 MPa $m^{1/2}$ in the base metal.

5. Residual stresses

Residual stresses are one characteristic of welding processes. They are caused primarily by the thermal welding cycle (local heating and rapid cooling).). The level of residual stress is influenced by the welding parameters. [26] report that they increase with increasing feed rate. [24] show that the change of the feed ratio changes the shape of the distribution and the maximum value of residual stresses in the longitudinal and transverse directions.

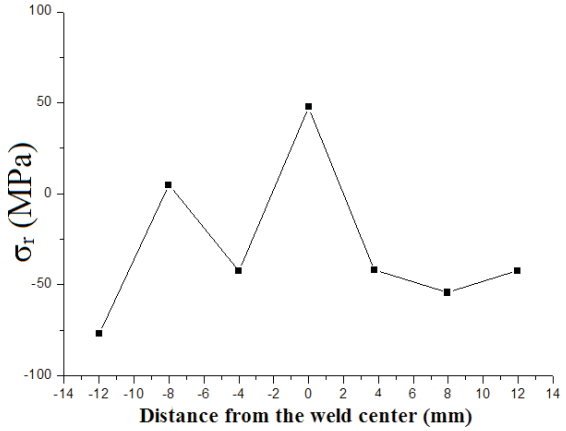

Figure 14 Residual stress profile in longitudinal direction respect to the welding one for the fatigue tested joints

The residual stresses have compressive character by approaching the weld line, changing to a tensile character in the weld zone from the heat affected one. It can be observed that the higher values of residual stresses are achieved in the advancing

side of the tool. The residual stresses values differences depend on the asymmetry of the FSW process; it is demonstrated by several finite element calculations that the higher deformation across the weld line are achieved in the retreating side of the tool when a clockwise direction is employed for the rotation.
The microstructure, hardness and residual stress distributions in the FSW are all complex. The studies in this work show each of them in three regions. These are the nugget region, the thermo mechanically affected zone and the HAZ. Each region has qualitatively or quantitatively distinct values of microstructure, hardness and residual stresses.
The nugget region has a fine recrystallised grain structure, with hardness values between 110 and 140 Hv1. within the nugget, residual stresses are low (8 MPa) parallel to the weld but large and tensile (174 MPa) perpendicular to the weld. Immediately outside the nugget, the thermo-mechanically affected zone consists of highly elongated and deformed grains, which comprise the softest (102 Hv1) part of the HAZ. This is the region with the highest recorded residual stress in the longitudinal direction of 264 MPa, and only 5 MPa in the transverse direction. Beyond 10–12 mm the structure is only heat affected and contains a parent plate grain structure. The hardness climbs rapidly throughout the thermo–mechanically affected zone reaching a maximum at about 20–25 mm from the PJL of almost 150 Hv1. Residual stresses in this region are compressive in both longitudinal and transverse directions, the transverse component being large _192 MPa and the longitudinal component small (_13 MPa).

6. Consequences of friction stir welding

The FSW welding process introduced significant changes in the microstructure through, in and around the joint. The impact of the process on the microscopic and macroscopic mechanical properties of the weld induces strong changes in the properties and the local and overall mechanical behavior of the bead weld. Many research works were carried out to define the behavior of welded joints FSW including quasi-static tensile and fatigue strength. Justifications are needed to explain why the initiation of fatigue cracks does not occur in the minimum microhardness zone? Why can they initiate cracks in the nugget and what is the role of the macrostructure, microstructure, hardness, state of precipitation and residual stresses in this phenomenon?
These tests make it possible to define, for each weld, critical areas to crack initiation. The resistance to rupture in HAZ is equal to the yield strength of the base metal. Therefore when there is a rupture in the HAZ, the base metal is just beginning to deform plastically. These results are the consequences of FSW.

7. Conclusion

The principle of FSW welding implies that the material at the interface of the plates to be assembled is kneaded. For this, it is necessary that the material be heated to a sufficient temperature, approximately 80% of its melting temperature to facilitate mixing. Very complex process FSW where the thermal, mechanical and

metallurgy remain coupled. The Purely analytical models have been developed as well as models based on methods without mesh, however, the finite element method is still the most widely used for modeling the FSW process.

This study allowed us to understand the mechanisms of FSW welding and determine in a first unlike the microstructure of welding these areas microhardness tests are used to confirm interpretations made on the heterogeneity of the structure of the solder joints.

Given the heterogeneity of FSW welding and especially that of the Nugget, it is necessary to know the areas likely to initiate the break during the various mechanical stresses (tensile and fatigue).

For a welding defect-free and properly polished, the crack propagation mechanism is related to three main elements: the residual stress, the crack initiation and the microstructure of the weld area. In the second step this study focused on the analysis of mechanical properties of the joint and the base metal.

This portion showed a decrease in the mechanical properties of the joint relative to the base metal.

The fatigue resistance under static and a FSW weld decreases linearly as a function of the maximum residual stress in certain conditions. The propagation velocity difference was attributed to the difference in microstructure around and in the weld zone rather than the existence of residual stresses.

Despite the fact that the residual stresses are minimal in FSW welds compared to welding of liquid phase processes, a significant quantity of these constraints may be observed, resulting in a critical deterioration of the seal and its performance in service.

A FSW weld contains residual stresses of compression and traction. The maximum residual stress is localized in the HAZ and the minimum residual stress is the compressive residual stress is localized in the side of advancing ZATM.

The width of the HAZ and low cooling rate produces a relatively small compressive residual stress in the weld.

The compressive stress may be useful to reduce crack propagation.

References

[1] **Thomas, W. M., Nicholas, E. D., Needham, J. C., Murch, M. G.,Temple-Smithm P. and Dawes, C. J.**: Friction–stir butt weldin, G.B. Patent No. 9125978.8, *International patent application*, No. PCT/GB92/02203, **1991**.

[2] **Ericsson, M. and Sandstrom, R.**: Influence of welding speed on the fatigue of friction stir welds and comparison with MIG and TIG, *International Journal of Fatigue*, 25, 12, 1379–1387, **2003**.

[3] **Thomas, W. M. and Nicholas, E.D.**: Friction stir welding for the transportation industries, *Mater. Des.*, 18(4-6), 269–73, **1997**.

[4] **Moreira, P. M. G. P., de Figueiredo, M. A. V. and de Castro, P. M. S. T.**: Fatigue behaviour of FSW and MIG weldments for two aluminium alloys, *Theor. Appl. Fract. Mech.*, 48, (2), 169–177, **2007**.

[5] **Moreira, P. M. G. P., de Jesus, A. M. P., Ribeiro, A. S. and de Castro, M. S. T.**: Fatigue crack growth in friction stir welds of 6082-T6 and 6061-T6 aluminium alloys: a comparison, *Theoretical and Applied Fracture Mechanics*, 50, 2, 81–91, **2008**.

[6] **Kobayashi, Y., Sakuma, M., Tanaka, Y. and Matsuoka, K.**: Fatigue strength of friction stir welding joints of aluminium alloy 6082 extruded shape, *Welding International*, 21, 1, 18–24, **2007**.

[7] **Costa, J. D., Ferreira, J. A. M. and Borrego, L. P.**: Influence of spectrum loading on fatigue resistance of AA6082 friction stir welds, *International Journal of Structural Integrity*, 2, 2, 122–134, **2011**.

[8] **Jata, K. V., Sankaran, K. K. and Ruschau, J. J.**: Friction–stir welding effects on microstructure and fatigue of aluminum alloy 7050-T7451, *Metallurgical and Materials Transactions* A, 31, 9, 2181–2192, **2000**.

[9] **Wan, L., Huang, Y. and Guo, W.**: Mechanical Properties and Microstructure of 6082–T6 Aluminum Alloy Joints by Self–support Friction Stir Welding, *State Key Laboratory of Advanced Welding and Joining*, Harbin Institute of Technology, Harbin 150001, China, **2014**.

[10] **Busu, G. and Irving, P. E.**: The role of residual stress and heat affected zone properties on fatigue crack propagation in friction stir welded 2024- T351 aluminium joints, *International Journal of Fatigue*, 25, 1, 77–88, **2003**.

[11] **Bouchouicha, B.**: Contribution à l'étude de la déchirure ductile et de la propagation des fissures en fatigue dans les joints soudés, PhD Thesis, Djillali Liabes University of Sidi Bel Abbes, **2007**.

[12] **Genevois, C.**: Genesis of the microstructures during friction stir welding of aluminium alloys of the serie 2000 and 5000 and resulting mechanical behavior, PhD Thesis, Institut National Polytechnique de Grenoble, **2004**.

[13] **Adamowski, J.**: Analysis of FSW welds made of aluminium alloy AW6082-T6, *Global Service Engineering R&D, Ansaldo Energia, Via N. Lorenzi*, 8, 16152 Genoa, Italy, **2007**.

[14] **Souto Grela, J., Blanco Viana, E. B., Martinez, D. and Piñeiro, E.**: Numerical simulation in welding process: optimizing structures with sequence and inertial study, *Matériaux & Techniques*, 100, 317–326, **2012**.

[15] **Feulvarch, E.**: Modélisation numérique du soudage par friction malaxage, Thèse de doctorat de l'Université de Saint Etienne, **2005**.

[16] **Merzoug, M.**: Etude paramétrique du soudage par friction malaxage, PhD Thesis, *Djillali Liabes University of Sidi Bel Abbes*, **2011**.

[17] Data from Mechanical laboratory of Lille (FRANCE), *Laboratoire de mécanique*, Université de Lille, FRANCE.

[18] **Harris D, Norman A. F.**: Properties of friction stir welded joints: a review of literature, *Progress report presented at the sixth PSG Meeting*, 17–18, **2003**.

[19] **Wan, L., Huang, Y., Guo, W., Lu,S. and Feng, J.**: Mechanical Properties and Microstructure of 6082-T6 Aluminum Alloy Joints by Self–support Friction Stir Welding, *State Key Laboratory of Advanced Welding and Joining*, Harbin Institute of Technology, Harbin 150001, China.

[20] **Scialpi, A., De Filippis, L. A. C. and Cavaliere, P.**: Influence of shoulder geometry on microstructure and mechanical properties of friction stir welded 6082 aluminium alloy, *Materials and Design*, 28, 4, 1124–1129, **2007**.

[21] **Svensson, L. E., Karlsson, L., Larsson, H., Karlsson, B., Fazzini, M. and Karlsson, J.**: Microstructure and mechanical properties of friction stir welded aluminium alloys with special reference to AA 5083 and AA 6082, *Science and Technology of Welding & Joining*, 5, 5, 285–296, **2000**.

[22] ASTM E8–04, Standard Test Methods for Tension Testing of Metallic Materials, **2004**.

[23] **Di, S., Yang, X., Luan, G., and Jian, B.**: Comparative study on fatigue properties between AA2024-T4 friction stir welds and base materials, *Materials Science and Engineering*, A 435-436:389–395, **2006**.

[24] **Lombard, H., Hatting, D. G., Steuwer, A. and James, M. N.**: Optimising FSW process parameters to minimise defects and maximise fatigue life in 5083-H321 aluminium alloy, *Eng. Fract. Mech.*, 75, 341–354, **2008**.

[25] **Bussu, G. and Irving, P. E.**: The role of residual stress and heat affected zone properties on fatigue crack propagation in friction stir welded 2024-T351 aluminium joints, *Int. J. Fat.*, 25, 1, 77–88, **2003**.

[26] **Peel, M., Steuwer, A., Preuss, M. and Withers, P. J.**: Microstructure, mechanical properties and residual stresses as a function of welding speed in aluminium AA5083 friction stir welds, *Acta Mater.*, 51, 4791–4801, **2003**.